J. Fluid Mech. (2004), *vol.* 502, *pp.* 17–40.
DOI: 10.1017/S0022112003007390 Printed in the United Kingdom

Thermoviscous stability of ice-sheet flows

By RICHARD C. A. HINDMARSH

British Antarctic Survey, Natural Environment Research Council, High Cross, Madingley Road, Cambridge CB3 OET, UK

(Received 12 June 2000 and in revised form 16 June 2003)

The shallow-ice approximation is used to analyse the normal-mode stability of long-wavelength, thermally coupled, free-surface flows of glaciers and ice sheets along infinite flow sections. The viscosity of the ice changes with temperature, and the ice is also thermally coupled with the bedrock. An assumption of quasi-uniform flow, where the downstream flux of mass and energy is assumed to be constant over relatively short wavelengths, permits vertical advection due to accumulation to be considered. The assumption allows realistic representation of the vertical velocity distribution and temperature distributions within the modelled flow. Nevertheless, the linearized equations are formally independent of the assumption of quasi-uniform flow. The linearized equations are Fourier-transformed over the horizontal plane and an algebraic eigenvalue problem constructed which considers the Fourier-transforms of the vertically varying temperature and thickness. The dependence of the eigenvalues on wavenumber, both parallel and orthogonal to flow, accumulation rate, geothermal heat flux, surface temperature and slope is computed. Extensive linearly unstable regimes where the base is well below melting point are found, which correspond only approximately to negative slopes in the flux/thickness relationship (supercritical zones). The most unstable parts of these regimes have finite along-flow wavelength, and have very long transverse wavelength. These modes are found to be more unstable in two senses: (i) they bifurcate for lesser thicknesses; (ii) they have greater growth rates. All computed wave velocities of unstable modes were downslope. Less unstable modes with short and medium transverse wavelengths are found which excite the temperature field only. Time constants range between ten and one thousand years. There is no strong evidence for stream-pattern formation through a thermoviscous instability mechanism.

1. Introduction

A normal-mode analysis of thermoviscously coupled shallow flows of ice is presented in this paper. MacAyeal (1992) has suggested that thermoviscous coupling is a significant factor in the dynamical variability of ice streams, and it has further been suggested that it is an essential component of a symmetry-breaking pattern-forming instability that leads to the formation of ice streams (Fowler & Johnson 1996; Payne & Dongelmans 1997). All previous glaciological analyses have been for zero wavenumber, and consequently cannot be used for understanding the spatial aspects of instabilities. Analogous geophysical flows do not seem to have been extensively analysed in this way, meaning that the relevance of the analysis extends beyond glaciology. The principal conclusion is that the most unstable mode has finite longitudinal wavelength, but possesses infinite transverse wavelength – a 'Squire's theorem result'. In consequence there is not a strong indication of ice streams emerging spontaneously through a symmetry-breaking instability.

The thermoviscous instability stems from the strong temperature dependence of the viscosity of ice and the sliding viscosity (sliding switches on at the pressure melting point of ice), while the flow of ice affects the temperature within an ice sheet or glacier, through advection and frictional dissipation. Early studies by Nye (1971), Clarke, Nitsan & Paterson (1977), Fowler & Larson (1980*a*), Yuen & Schubert (1979) and Yuen, Saari & Schubert (1986) considered the stability of thermo-mechanically coupled flows down an infinite plane. These studies focused on the role of multiple steady states in the temperature and in the ice flow, introduced by coupling of the internal heating and the temperature, in determining the qualitative dynamics. Fowler & Larson (1980*b*) and Yuen & Schubert (1979) both suggest that these flows are linearly stable, but unstable in the presence of finite-amplitude perturbations. In contrast, both Nye (1971) and Clarke *et al.* (1977) found linear instabilities. All these authors considered the vertical dimension only, and none therefore performed a normal-mode analysis which included finite horizontal wavelengths. Moreover, those who did consider linear stability did not fully couple their linearized temperature evolution equations with the ice-thickness evolution equation. An extensive review is found in Hutter (1983, Chap. 3), where the omissions of previous studies are discussed. Some of these issues are addressed here, in particular by: (i) considering finite wavelengths in two horizontal dimensions; and (ii) considering the coupling between the temperature and the evolving free surface.

Following on from these earlier works, a large number of numerical experiments have considered more realistic ice-sheet geometries (MacAyeal 1992, 1993; Payne 1995; Greve & MacAyeal 1996; Pattyn 1996; Marshall & Clarke 1997). The results suggest that the coupling between the temperature-dependent viscosity and sliding of ice sheets, dissipation and heat transport can lead to situations where limit cycles or more complex behaviour (in an infinite-dimensional phase space) can occur. Numerical experiments (e.g. Fowler & Johnson 1996, Payne & Dongelmans 1997) suggest that when two horizontal dimensions are considered, more complex, finger-like, structures emerge. Numerical results are justified by physically-motivated plausibility reasoning (Payne *et al.* 2000), although some of this reasoning may be over-simplified (Hindmarsh 2001). The numerical calculations reported above simulate complex dynamical phenomena, and some more rigorous mathematical confirmation of the validity of at least a subset of the solutions is needed. An aim of this paper is to relate the numerical solutions to the earlier analytical and semi-analytical studies. An important caveat is that the stability analysis presented in this paper does not deal with cases where significant horizontal variations of the base-case fields (e.g. the bedrock topography, the temperature) are involved. It is conceivable that these long-wavelength horizontal variations significantly modulate the stability of ice sheets.

Vertical advection of ice replenished by snowfall affects temperature fields within ice. A device introduced by Clarke *et al.* (1977) is used, which permits consistent consideration of vertical advection whilst retaining a horizontally uniform zeroth-order flow on the infinite plane. Mass is added to the upper surface as accumulation on the surface of an ice sheet; however, the horizontal velocity or thickness are assumed not to increase significantly over length scales of interest, such that we can treat a base case of uniform flow. This is the assumption of *quasi-uniform flow*. The same argument applies to the heat added to the system through geothermal heating and internal dissipation, meaning that the temperature profile is assumed to remain unchanged downstream. If the accumulation rate is zero, the quasi-uniformity becomes uniformity.

The significance of the assumption of quasi-uniform flow is that by permitting vertical transport, one creates vertical distributions of temperature that are realistic, for example the basal boundary layer (e.g. Morland 1984). It turns out that formally, the perturbation equations are independent of the accumulation rate (and thus whether we have assumed uniformity or quasi-uniformity), although the accumulation rate does (and must) affect the zeroth-order solution. An important *a posteriori* result is that including vertical advection does not significantly affect the qualitative dynamics.

This study highlights the observation that thermomechanical coupling occurs in a number of different ways. (i) *Thermoviscous dissipative coupling*. Heating within the ice depends upon the product of strain rate and deviator stress. The strain rate depends upon the stress and the temperature owing to the temperature-dependence of the viscosity and the sliding (interface) viscosity. It is purely a local effect due to viscous heating. (ii) *Thermokinematical coupling*. The dependence of the flow rate on the viscosity (itself affected by temperature) introduces a coupling between temperature and velocity. Changes in the velocity affect advection, which in turn affects the temperature distribution and the geometry of the ice sheet. This changes the geometry of the domain on which the heat equation is solved. This coupling occurs independently of whether there is significant viscous heating or not. (iii) *Free-surface-driven dissipative coupling*. As in the previous case, the dependence of the flow rate on the viscosity (itself affected by temperature) introduces a coupling between temperature and velocity. Such changes in the velocity affect the free-surface geometry. This is turn affects the stresses within the ice, which alter the dissipative heating. This coupling occurs independently of any other heat transport mechanisms. (iv) *Glacier–lithosphere thermal coupling,* which is a direct coupling between the temperature fields in the ice and the rock. It is known to be a quantitatively significant effect (Ritz 1987). All of these couplings are included in this study.

The mechanical model used here is the shallow-ice approximation (Hutter 1983) which omits stresses apart from the horizontal plane shear components. These omissions can be important when the flow is streamed, and symmetry strongly broken. However, this paper is primarily concerned with the inception of symmetry breaking, or flows where the symmetry is weakly broken, for example in the upstream areas (Bamber, Vaughan & Joughin 2001).

To this end, a base case of a uniform flow down a slope is constructed, and the coupled flow and thermal solutions are then perturbed. The stability of the flow is investigated through solution of a numerical eigenvalue problem. This is expressed in terms of the Fourier coefficients, calculated from the Fourier transform over the horizontal plane of the ice thickness and the temperature (which depends upon the vertical coordinate). Cases are investigated where flow is by internal deformation; in addition, the effect of temperature-dependent sliding is simulated by introducing an activation energy for sliding. This construction allows an increase in velocity over a narrow temperature range centred on the melting point. It can be justified by appeal to theoretical predictions of sub-temperate basal sliding (Fowler 1986) or by empirical/theoretical considerations of molten patches (Hughes 1988; Kleman, Hättestrand & Clarhäll 1999).

A search for stable and unstable regimes is performed over a parameter space defined by the ice thickness, the slab slope, the heat transport equation boundary conditions, the accumulation rate and the two wavelength components. Two types of instability are found at finite wavelength.

Instabilities in thin-film flows other than glaciers have been studied for some time. Two particular lines of enquiry are relevant here. Firstly, the thermal coupling induces large variations in viscosity. Viscosity stratification can destabilize shear flows (Yih 1967; Hooper & Boyd 1983). These works consider perturbations to the Orr–Sommerfeld equation, and instabilities can exist for all non-zero Reynolds numbers, with the magnitude of the instability being proportional to the Reynolds number. At freezing point, under a deviatoric stress of 10^5 Pa, the viscosity of ice is around 10^{13} Pas, and for flows at 100 myr^{-1} of thickness 1000 m, a typical Reynolds number is around 10^{-13}. This gives times cales for evolution of the Yih modes very much longer than the lifetime (10^5 to 10^7 a) of an average ice sheet, meaning that this source of instability can be ignored in the present analysis.

Thin-film researchers have also looked at thermal effects (Reisfeld & Bankoff 1992; Oron, Davis & Bankoff 1997; Davis 2000). These have been for flows a few millimetres thick at most, where temperature changes can occur much more quickly than changes in the free-surface geometry, and the thermal and flow problems decouple, unlike the present case. A more closely analogous case is of hot lava (Balmforth & Craster, 2000), which is of interest because a fingering instability is found. This study differs from the present case in two important ways: the temperature is independent of the vertical coordinate, and viscous heating can be ignored. This diversity of studies illustrates the likely complexity of thermoviscous coupling.

2. Model formulation

The normal-mode analysis linearizes about a base case of quasi-uniform flow of ice of fine thickness down the infinite plane, with recharge by accumulation. The ice overlies a half-space of rock. It is supposed that the wavelengths considered are small enough for the flow not to increase substantially over this length. Boundary conditions consist of a supply of heat to the base of the rock or the ice, and a prescribed surface temperature. Dissipative heating is considered, and the dependence of ice and sliding viscosity on temperature are included when solving the nonlinear equation coupling temperature and ice flow. Momentum terms are vertically integrated using the shallow-ice approximation. Specific examples of base flows are discussed further in § 3. The normal-mode analysis yields a linear coupled eigenvalue problem in the thickness of the ice, the temperature in the ice and the temperature in the bedrock. After basic definitions, the eigenvalue problem is presented in § 2.3, followed by the details of its derivation.

2.1. *Governing equations, scaling, linearization and Fourier transform*

The setup of flow down an infinite plane is illustrated in figure 1. Dimensional quantities are represented by a tilde, non-dimensional quantities without a tilde. Fourier transforms are represented by a caret. The coordinates are $(\tilde{x}, \tilde{y}, \tilde{z})$, where $\tilde{z}$ is perpendicular to the base plane and $\tilde{x}$ is in the zeroth-order flow direction. The $\tilde{z}$-direction is called 'vertical' and the $\tilde{\boldsymbol{r}} = (\tilde{x}, \tilde{y})$ plane 'horizontal'. The thickness of the ice is given by $\tilde{z} = \tilde{H}(\tilde{\boldsymbol{r}}, \tilde{t})$, while the upper and lower surfaces are given by $\tilde{z} = \tilde{s}(\tilde{\boldsymbol{r}}, \tilde{t})$, $\tilde{z} = \tilde{b}(\tilde{\boldsymbol{r}}, \tilde{t})$ respectively, and $\tilde{t}$ represents time. Superscripts (s), (b) indicate evaluation at the surface or base respectively. The surface $\tilde{z} = \tilde{b}(\tilde{\boldsymbol{r}}, \tilde{t})$ forms an upper surface for the bedrock. The operators ∇_{H}, $\nabla_{\mathrm{H}} \cdot$, represent the horizontal gradient and divergence respectively.

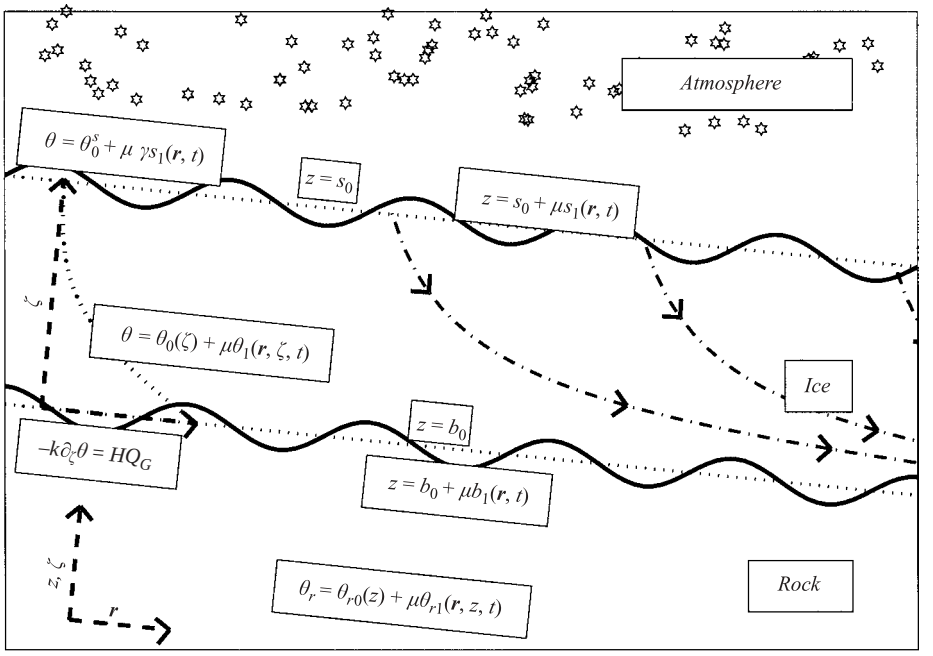

FIGURE 1. Coordinate sytem for flow down an infinite plane with perturbed upper and lower surfaces, streamlines and a typical zeroth-order vertical temperature distribution (see axes on the left). One possible basal boundary condition (no sliding, no thermal inertia in bedrock) is indicated. Note the two vertical coordinates z, ζ and the vector horizontal coordinate $\boldsymbol{r} = (x, y)$ where x is in the downslope direction and y represents transverse flow. The normalized coordinate $\zeta \equiv (z - b)/(s - b)$ is used within the ice.

The three-dimensional velocity field is conveniently represented by the vertical velocity $\tilde{w}$ and the horizontal velocity vector $\tilde{\boldsymbol{u}} = (\tilde{u}_x, \tilde{u}_y)$, and we also use $\tilde{\boldsymbol{v}} = (\tilde{u}_x, \tilde{u}_y, \tilde{w})$. The volume flux $\tilde{\boldsymbol{Q}} = \int_{\tilde{b}}^{\tilde{s}} \tilde{\boldsymbol{u}}\mathrm{d}z$ is used frequently throughout the paper.

The governing equations, which apply to all $\tilde{\boldsymbol{r}}$, are

$$\nabla_{\mathrm{H}} \cdot \tilde{\boldsymbol{u}} + \partial_{\tilde{z}}\tilde{w} = 0, \qquad \tilde{b}(\tilde{\boldsymbol{r}}, \tilde{t}) \leqslant \tilde{z} \leqslant \tilde{s}(\tilde{\boldsymbol{r}}, \tilde{t}), \tag{2.1a}$$

$$\partial_{\tilde{t}}\tilde{s} + \tilde{\boldsymbol{u}} \cdot \nabla\tilde{s} = \tilde{w} + \tilde{a}, \qquad \tilde{z} = \tilde{s}(\tilde{\boldsymbol{r}}, \tilde{t}), \tag{2.1b}$$

$$\nabla \cdot \tilde{\sigma} + \tilde{\rho}\tilde{\boldsymbol{g}} = \boldsymbol{0}, \qquad \tilde{b}(\tilde{\boldsymbol{r}}, \tilde{t}) \leqslant \tilde{z} \leqslant \tilde{s}(\tilde{\boldsymbol{r}}, \tilde{t}), \tag{2.1c}$$

$$\tilde{\boldsymbol{\sigma}}^{(s)} \cdot \boldsymbol{n}^{(s)} = \boldsymbol{0}, \qquad \tilde{z} = \tilde{s}(\tilde{\boldsymbol{r}}, \tilde{t}), \tag{2.1d}$$

$$\left.\begin{array}{rl} \tilde{\boldsymbol{v}}^{(b)} = \boldsymbol{0}, & \text{frozen bed,} \\ \text{equation (2.4) } \& \ \boldsymbol{n}^{(b)} \cdot \tilde{\boldsymbol{v}}^{(b)} = \boldsymbol{0}, & \text{melting bed,} \end{array}\right\} \qquad \tilde{z} = \tilde{b}(\tilde{\boldsymbol{r}}, \tilde{t}), \tag{2.1e}$$

$$\partial_{\tilde{t}}\tilde{\theta} + \tilde{\boldsymbol{u}} \cdot \nabla_{\mathrm{H}}\tilde{\theta} + \tilde{w}\partial_{\tilde{z}}\tilde{\theta} = \tilde{\kappa}\nabla^2\tilde{\theta} + \frac{1}{\tilde{\rho}\tilde{c}}\tilde{D}, \qquad \tilde{b}(\tilde{\boldsymbol{r}}, \tilde{t}) \leqslant \tilde{z} \leqslant \tilde{s}(\tilde{\boldsymbol{r}}, \tilde{t}), \tag{2.1f}$$

$$\tilde{\theta}^{(s)} - \tilde{\theta}^{s} = 0, \qquad \tilde{z} = \tilde{s}(\tilde{\boldsymbol{r}}, \tilde{t}), \tag{2.1g}$$

$$K_r\nabla\tilde{\theta}_r^{(b)} \cdot \boldsymbol{n}^{(b)} - \tilde{\boldsymbol{v}}^{(b)} \cdot \tilde{\boldsymbol{\sigma}}^{(b)}\boldsymbol{n}^{(b)} = K_i\nabla\tilde{\theta}^{(b)} \cdot \boldsymbol{n}^{(b)} \qquad \tilde{z} = \tilde{b}(\tilde{\boldsymbol{r}}, \tilde{t}), \tag{2.1h}$$

$$\partial_{\tilde{t}}\tilde{\theta}_r = \tilde{\kappa}_r\nabla^2\tilde{\theta}_r, \qquad \tilde{z} \leqslant \tilde{b}\left(\tilde{\boldsymbol{r}}, \tilde{t}\right), \tag{2.1i}$$

$$\tilde{\theta}^{(b)} = \tilde{\theta}_r^{(b)}, \qquad \tilde{z} = \tilde{b}\left(\tilde{\boldsymbol{r}}, \tilde{t}\right), \tag{2.1j}$$

$$-\tilde{K}_r\partial_{\tilde{z}}\tilde{\theta}_r = \tilde{Q}_{G,} \qquad \tilde{z} \to -\infty. \tag{2.1k}$$

Here (2.1*a*) expresses conservation of mass in the ice; (2.1*b*) is the free-surface kinematic condition, where $\tilde{a}$ is accumulation rate of ice, expressed as a volume rate per unit area; (2.1*c–e*) describe conservation of momentum in the ice, where $\tilde{\boldsymbol{\sigma}}$ is the stress tensor, $\tilde{\rho}$ is the density of ice, $\tilde{\boldsymbol{g}} = \tilde{g}(\varepsilon, 0, -1)$ is the gravitational acceleration vector (note the existence of a downstream body force which drives the flow) and $\boldsymbol{n}$ is the normal vector at the indicated surface; (2.1*f–h*) represent conservation of heat in the ice, where $\tilde{\theta}, \tilde{\theta}_r$ are the temperatures in the ice and rock respectively, $\tilde{\theta}^s$ is the prescribed surface temperature, $\tilde{\kappa}$ is the thermal diffusivity of ice, $\tilde{c}$ is the specific heat capacity, $\tilde{D} = \frac{1}{2}\mathrm{trace}(\tilde{\boldsymbol{\tau}} \cdot \tilde{\mathbf{e}})$ is the dissipation, $\tilde{\boldsymbol{\tau}}$ is the deviatoric stress and $\tilde{K}_i$, $\tilde{K}_r$ are the thermal conductivities of ice and rock respectively; and (2.1*i–k*) represent conservation of heat in the rock, where $\tilde{\kappa}_r$ is the thermal diffusivity of the rock and $\tilde{Q}_G$ is the geothermal heat flux. A reduced form of these equations will be described and used.

The constitutive relations have two parts. (i) A nonlinear viscous relationship within the ice

$$\tilde{\mathbf{e}} = \tilde{A}_c R(\tilde{\theta}, \tilde{p}) \, |\tilde{\tau}|^{n-1} \, \tilde{\boldsymbol{\tau}}, \tag{2.2}$$

where $\tilde{\mathbf{e}}$ is the strain-rate tensor, the deviatoric stress tensor $\tilde{\boldsymbol{\tau}}$ has a second invariant $\tilde{\tau}$, defined by

$$\tilde{\tau}^2 = \tfrac{1}{2}\mathrm{trace}(\tilde{\boldsymbol{\tau}}^2), \tag{2.3}$$

$\tilde{p}$ is the pressure, n is the Glen index, $\tilde{A}_c$ is a rate factor and R is a dimensionless function which expresses the dependence of the flow relation on scalars such as temperature and pressure. The temperature dependence in this paper is modelled through Arhenuis-type relationships. (ii) An isotropic sliding relation of the form

$$\tilde{\boldsymbol{u}}_{\parallel}^{(b)} = \tilde{A}_s S(\tilde{\theta}, \tilde{p}) \left| \tilde{\boldsymbol{T}}^{(b)} \right|^{\ell - 1} \tilde{\boldsymbol{T}}^{(b)}, \tag{2.4}$$

where $\tilde{\boldsymbol{u}}_{\parallel}^{(b)}$ is the sliding velocity, $\tilde{\boldsymbol{T}}^{(b)}$ is the basal tangential traction, ℓ is the sliding index, $\tilde{A}_s$ is the sliding rate factor and $S(\tilde{\theta}, \tilde{p})$ is a dimensionless function expressing the dependence of sliding velocity on temperature and pressure. The constitutive relationships are discussed in the Appendix, § A.2.

Thicknesses H and elevations z, s, b are scaled by $\tilde{H}_*$(asterisk subscripts imply a scale magnitude), and horizontal positions $\boldsymbol{r} = (x, y)$ are scaled by

$$\tilde{L}_* = \tilde{H}_* / \varepsilon. \tag{2.5}$$

Note that the downstream body force component ε has been chosen to be the aspect ratio of the flow as well. This choice ensures that the downstream body force in the scaled system is unity, but requires ε^2 be small in order to use the shallow-ice approximation.

Dimensionless field quantities within the ice are expressed in a normalized vertical coordinate ζ defined by

$$0 \leqslant \zeta = \tilde{H}^{-1}(\tilde{z} - \tilde{b}) = H^{-1}(z - b) \leqslant 1. \tag{2.6}$$

Hindmarsh & Hutter (1988) and Hindmarsh (1999) write out the associated differential transforms. In physical units the operators $\nabla_{\mathrm{H}} \cdot, \nabla_{\mathrm{H}}$ act in the $(\tilde{\boldsymbol{r}}, \tilde{z})$ coordinate system, while in the dimensionless system they act in the in $(\boldsymbol{r}, \zeta)$ system. Pressure and stress are scaled by $\tilde{\rho}\tilde{g}\tilde{H}_*$, where $\tilde{g} = |\tilde{\boldsymbol{g}}|$ is the acceleration due to gravity. In dimensionless form, the gravity vector $\boldsymbol{g}$ has components $(\varepsilon, 0, -1)$ where $\varepsilon^2 \ll 1$. This is the same quantity as used in (2.5). The deviator stresses $\boldsymbol{\tau}$ are scaled by $\varepsilon\tilde{\rho}\tilde{g}\tilde{H}_*$. The temperature in the ice $\theta(\boldsymbol{r}, \zeta, t)$ (note the dependence on the normalized

vertical coordinate) and in the rock $\theta_r(\boldsymbol{r}, z, t)$ are scaled by the temperature magnitude $\tilde{\theta}_*$. The accumulation rate a and the vertical velocity w are scaled by $\tilde{a}_* = \tilde{u}_* \tilde{H}_* / \tilde{L}_*$, the flux has scale given by $\tilde{q}_* = \tilde{u}_* \tilde{H}_*$ and time is scaled by $\tilde{t}_* = \tilde{L}_* / \tilde{u}_*$. The choice of $\tilde{u}_*$ depends on the flow mode and is discussed in § A.2, where scalings for A_c and A_s may also be found.

Advantage is taken of the small aspect ratio of the problem to simplify the governing equations (2.1) by applying the standard (Hutter 1983; Morland 1984; Fowler 1992) shallow-ice approximation (SIA). The SIA expands the governing equations in terms of the aspect ratio ε, simplifying the mass and momentum conservation equations (2.1*a–e*) so that the velocity and flux can be computed directly by quadrature, using equations (A 18) and (A 19). Details are given in the Appendix. The relevant field variables are subsequently linearized with a small parameter μ about a base-case solution (steady uniform flow down an infinite plane), e.g.

$$H = H_0 + \mu H_1(\boldsymbol{r}, t), \quad b = \mu b_1(\boldsymbol{r}, t), \quad \boldsymbol{Q} = \boldsymbol{Q}_0 + \mu \boldsymbol{Q}_1(\boldsymbol{r}, t), \tag{2.7}$$

etc., and are used to derive a set of zeroth- and first-order equations expressing conservation of mass, momentum and energy.

A Fourier transform in the horizontal plane is then applied to the first-order equations, and the first-order fields can be expressed as plane waves

$$H_1 = \mathrm{Re}\{\hat{H}_1 \exp(\lambda t - \mathrm{i}\boldsymbol{k}\cdot\boldsymbol{r})\}, \quad \theta_1 = \mathrm{Re}\{\hat{\theta}_1(\zeta) \exp(\lambda t - \mathrm{i}\boldsymbol{k}\cdot\boldsymbol{r})\}, \tag{2.8}$$

etc., where λ is the eigenvalue, the wavenumbers are given by $\boldsymbol{k} = (k_x, k_y)$ and the caret indicates the Fourier coefficient of the transform over the $\boldsymbol{r}$-plane only.

2.2. *The base flow*

The scaling is specified to ensure that H_0 and as many as possible of the other zeroth-order quantities are unity. In particular $\boldsymbol{Q}_0 = (1, 0)$, and the zeroth-order horizontal velocities $\boldsymbol{u}_0$ are given by (A 19).

At zeroth order the heat equations (2.1*f–k*) are

$$\psi_0 \partial_\zeta \theta_0 = \beta \partial_\zeta^2 \theta_0 + \alpha \partial_\zeta u_{0x} (1 - \zeta), \qquad 0 \leqslant \zeta \leqslant 1, \tag{2.9a}$$

$$\varpi u_{0x}^{(b)} - K_r \partial_z \theta_{r0}^{(b)} = -\partial_\zeta \theta_0^{(b)} \qquad \zeta = 0, \tag{2.9b}$$

$$\theta_0(\zeta = 1) = \theta_0^s, \qquad \zeta = 1, \tag{2.9c}$$

$$\kappa_r \partial_z^2 \theta_{r0} = 0, \qquad z < b, \tag{2.9d}$$

$$-K_r \partial_z \theta_{r0} = Q_G, \qquad z \to -\infty, \tag{2.9e}$$

where ψ_0 is defined in (2.14) and the parameters β, α, ϖ are dimensionless order-unity thermal parameters given in (A 27). The spatial coordinates ζ, z are the independent variables of this equation. In practical computations, the flux is treated as the target variable ($\tilde{q}_* = \tilde{H}_* \tilde{u}_*$ is specified), and the thickness scale $\tilde{H}_*$ is adjusted until a steady solution can be found. This process of adjustment is somewhat complicated, as the thickness scale and flux scale imply a required velocity scale, which is constructed by scaling the relevant rate factors through (A 6) (internal deformation) or (A 12) (sliding). However, these rate-factor scales depend upon the zeroth-order temperature field obtained from solution of (2.9), which implies an iterative procedure in obtaining the thickness scale and temperature field consistent with the target flux. This can proceed because the thickness and velocity scales completely determine the parameters $\kappa, \kappa_r, \alpha, \varpi$ used in the zeroth-order equations (2.9). The sliding velocity $u_{0x}^{(b)}$ is either

0 (internal deformation) or 1 (sliding) by construction, and

$$\partial_\zeta u_{0x} = (n+2)\frac{R(\theta_0)}{R_0} \tag{2.9f}$$

is the zeroth-order statement of the scaled shear relationship (A 10).

2.3. *The eigenvalue problem*

The first-order equations lead to the formulation of an eigenvalue problem in $(\hat{H}_1, \hat{\theta}_1, \hat{\theta}_{1r})$, presented below in equations (2.10)–(2.13). The derivation of the eigenproblem is outlined in the Appendix, presenting the momentum balance, the constitutive relationships, the computation of the flow fields, the material balance and the heat balance. The labelling within the equations below is to facilitate discussion in § 4.2. Specifically, the eigenproblem comprises the following. (i) The scalar equation for the ice thickness

$$\lambda\hat{H}_1 = \mathrm{i}k_x\left(\overbrace{(m+\nu\mathrm{i}k_x)\hat{H}_1}^{\text{(iii),(iv)}} + \nu\mathrm{i}k_x\hat{b}_1 + \overbrace{\mathscr{C}[\hat{\theta}_1;1]}^{\text{(ii),(iv)}}\right) - k_y^2\hat{s}_1, \tag{2.10}$$

which is obtained from (A 20) and (A 24). The quantity $\mathscr{C}[\hat{\theta}_1;\cdot]$ is a functional expressing the dependence of the (sliding) viscosity on the temperature, defined in (A 21), and m, ν are constants which depend on the constitutive relationships and the flow mode of the ice-sheet, defined in (A 15). (ii) The ice temperature field equation

$$\lambda\hat{\theta}_1 - \overbrace{\mathrm{i}u_{0x}k_x\hat{\theta}_1}^{\text{(v)}} + \psi_0\frac{\mathrm{d}\hat{\theta}_1}{\mathrm{d}\zeta} + \partial_\zeta\theta_0\hat{\psi}_1 = \beta\frac{\mathrm{d}^2\hat{\theta}_1}{\mathrm{d}\zeta^2} + G\hat{H}_1 + \overbrace{\alpha\hat{D}_1}^{\text{(ii)}}, \quad 0<\zeta<1, \tag{2.11a}$$

$$G \equiv \psi_0\partial_\zeta\theta_0 - 2\beta\partial_\zeta^2\theta_0, \tag{2.11b}$$

with top and bottom boundary conditions

$$\hat{\theta}_1 - \gamma\hat{s}_1 = 0, \qquad \zeta = 1, \tag{2.12a}$$

$$\frac{\mathrm{d}\hat{\theta}_1}{\mathrm{d}\zeta} = -\partial_\zeta\theta_0^{(b)}\hat{H}_1 - \frac{K_r}{K_i}\partial_z\hat{\theta}_{r1} + \varpi u_{0x}^{(b)}\left(F\hat{s}_1 - \overbrace{\mathscr{C}[\hat{\theta}_1,1]}^{\text{(ii)}}\right), \quad \zeta = 0, \tag{2.12b}$$

$$F \equiv (\nu+1)(1+\mathrm{i}k_x). \tag{2.12c}$$

(iii) The bedrock temperature field equation

$$\lambda\hat{\theta}_{r1} = \beta_r\partial_z^2\hat{\theta}_{r1}, \qquad -\infty < z \leqslant b, \tag{2.13a}$$

$$-K_r\partial_z\hat{\theta}_{r1} = 0, \qquad z\to-\infty, \tag{2.13b}$$

$$\hat{\theta}_{r1} - \hat{\theta}_1 = 0, \qquad z = b. \tag{2.13c}$$

Equations (2.11)–(2.13) are obtained directly by linearization of (A 25). The parameters $\beta, \alpha, \varpi, \beta_r$ are dimensionless order-unity thermal parameters given in (A 27); γ is the lapse rate; $\partial_\zeta\theta_0^{(b)}$ is given in (2.9*b*); the heat equation whose solution yields θ_0 is also given in (2.9), and ψ_0 and $\hat{\psi}_1$ are quantities related to the vertical velocity in the ice,

$$\psi_0 \equiv -a_0\int_0^\zeta u_{0x}\,\mathrm{d}\zeta', \quad \hat{\psi}_1 \equiv -\mathrm{i}\boldsymbol{k}\cdot(\zeta\,\hat{\boldsymbol{Q}}_1 - \hat{\boldsymbol{q}}_1), \tag{2.14}$$

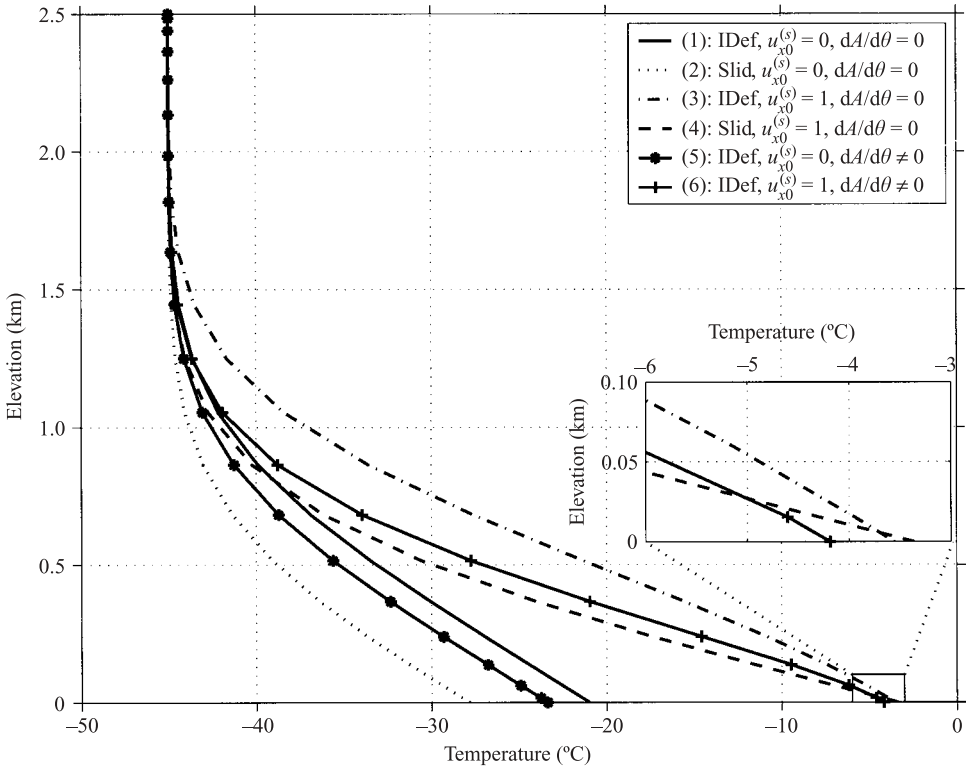

FIGURE 2. Zeroth-order steady-state solutions for no dissipation ($u_{x0}^{s} = 0$) and dissipation ($u_{x0}^{s} = 1$), sliding (slid) and internal deformation (IDef) with thermoviscously uncoupled ($dA/d\theta = 0$) and coupled ($dA/d\theta \neq 0$) flow. The zoom shown in the inset has same data aspect ratio as the main plot, so that slopes can be directly compared. The dimensionless diffusivity $\beta = 0.04$.

where the accumulation rate is denoted by a_0, and the zeroth-order downstream velocity u_{0x} is defined in (A 19). The quantity $\hat{\psi}_1$ is defined in terms of the horizontal gradient of the first-order fluxes $(\hat{\boldsymbol{Q}}_1, \hat{\boldsymbol{q}}_1)$ given in (A 20). The dissipations are given by $D_0 = 2A_c R(\theta_0)(1-\zeta)^{n+1}$ and

$$\hat{D}_1/D_0 = F\hat{H}_1 + \frac{\dot{R}(\theta_0)}{R(\theta_0)}\hat{\theta}_1. \tag{2.15}$$

The constitutive parameters A_c and R are defined in § A.2.

3. Multiple solutions of the zeroth-order equation

The parameters of the zeroth-order steady problem are the accumulation rate, the ice thickness, the geothermal heat flux, the surface temperature and the longitudinal component of gravity. The dimensionless system has no fewer free parameters. It is therefore convenient to present results in physical units. Examples of solutions to the zeroth-order system (2.9) may be found in Paterson (1994) and Hindmarsh (1999). Solutions were obtained numerically using finite-difference methods. Figure 2 show some solutions for cases where there is viscous heating and where there is thermoviscous coupling as well as more standard cases. Note the existence of a boundary layer, and the low sensitivity of the thickness of the boundary layer to

Parameter	Combination 1	Combination 2
$\tilde{a}$	$(-5, 0, 0.03, 0.1, 0.3)\,\mathrm{myr}^{-1}$	$(-5, 0, 0.03, 0.1, 0.3)\,\mathrm{myr}^{-1}$
$\tilde{Q}_G$	$0.06\,\mathrm{W\,m}^{-2}$	$(0.04, 0.08)\,\mathrm{W\,m}^{-2}$
$\tilde{\theta}_s$	$-25^{\circ}\mathrm{C}$	$(-40, -10)^{\circ}\mathrm{C}$,
ε	$(10^{-4}, 10^{-3}, 2\times10^{-3}, 5\times10^{-3}, 10^{-2}, 10^{-1})$	2×10^{-3}

TABLE 1. Parameter study in the accumulation rate $\tilde{a}$, the geothermal heat flux $\tilde{Q}_G$, the surface temperature $\tilde{\theta}_s$ and the x-component of gravity ε. The parameter study comprised the sets of all possible combinations in each of the two columns.

mode of deformation. Morland (1984) carries out a scale analysis of the boundary layer which is consistent with these finding.

A parameter study of zeroth-order solutions comprising 50 combinations of the parameters $\tilde{a}$, $\tilde{Q}_G$, $\tilde{\theta}^s$ and ε, given in table 1, was carried out. For each combination of the parameters, steady solutions were computed for different thicknesses $\tilde{H} \geqslant 0$ for the range $\tilde{\theta}_0^{(b)} = [\tilde{\theta}_0^{(s)}, \tilde{\theta}_m]$. In general, the discharge and basal temperature are bi-valued functions of thickness. Previous workers have found tri-valued solutions, with an additional fast flow branch, where the flux increases with thickness. This corresponds to a change in the basal boundary condition where the basal temperature has reached the melting point. In this third branch, the flux increases with thickness primarily because the basal traction increases with thickness. This branch is not considered in this paper.

For given combinations of accumulation rate, ice thickness, geothermal heat flux and surface temperature, there is frequently a maximum thickness. Figure 3 shows plots of the discharge Q_H, considered as a function of the zeroth-order thickness $\tilde{H}_*$, for six different values of the plane slope ε. The subscript H indicates that the dependent variable is being considered as a function of the thickness. The geothermal heat flux in these examples was $0.06\,\mathrm{W\,m}^{-2}$ and the surface temperature was $-25^{\circ}\mathrm{C}$. An observation from the computations is that the flux and basal temperature vary monotonically, which means that the basal temperature is also a two-valued function of thickness, with turning points occurring for the same thickness as for the discharge/thickness curves. Where the slopes are relatively small, the flux and basal temperature vary monotonically with the thickness, but for $\varepsilon \geqslant 0.002$ the functions becomes bi-valued. This is particularly true for larger positive accumulation rates, while the case with ablation only exhibits bi-valuedness for $\varepsilon = 0.1$. Other studies show that there is very little dependence of the shape of the curve on geothermal heat flux, and that warmer surface temperatures can suppress the emergence of bi-valuedness.

Informally, systems are held to be unstable when the slopes of Q_H or $\theta_H^{(b)}$ are negative; this would be true if the evolution equations had one evolving mode. The results of the next section are anticipated by pointing out that unstable thicknesses, as revealed by a normal-mode analysis, do not correspond to places where the these slopes are negative, and in fact such negative slopes are neither necessary nor sufficient for instability.

4. Computation of the normal modes.

The eigenvalue problem is solved by discretizing equations (2.11), (2.12), (2.13), yielding an algebraic eigenvalue problem. The resulting matrix operator contains one row corresponding to $\hat{H}_1$, and a number of rows corresponding to the temperature

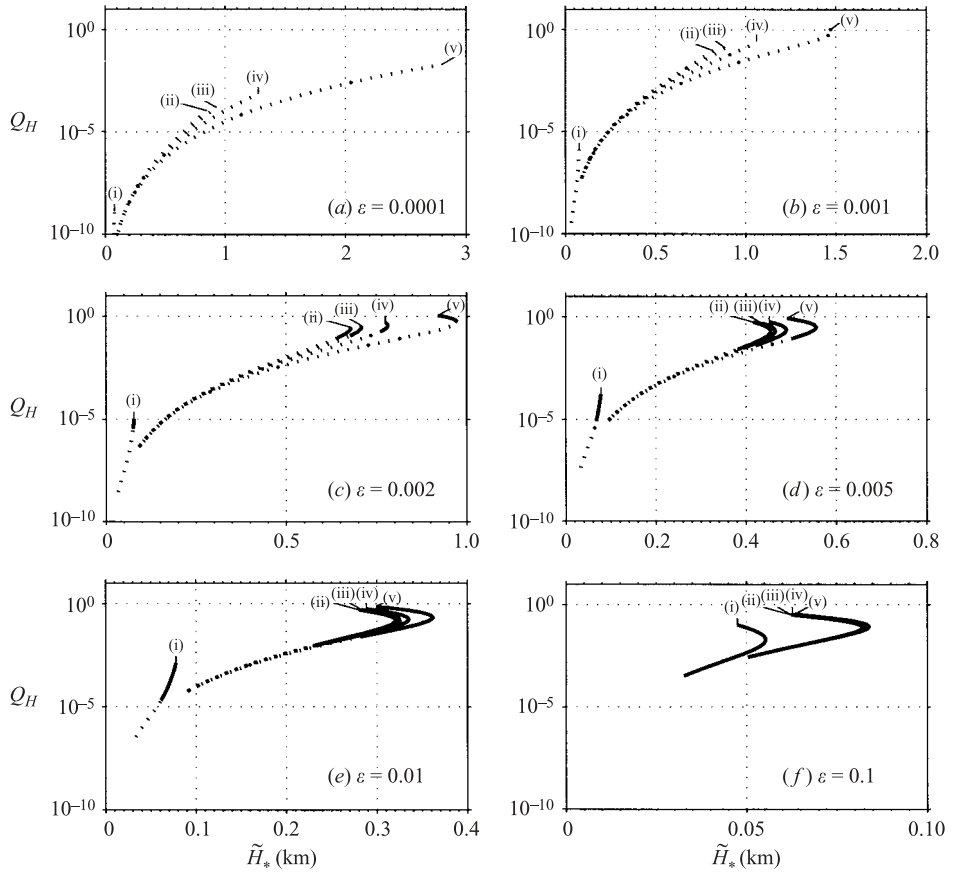

FIGURE 3. Flux thickness (i.e. $Q_H(H)$) diagrams for flow by internal deformation with $\theta^{(s)} = -25°\mathrm{C}$, $Q_G = 0.06\,\mathrm{W\,m^{-2}}$. In $(a–f)$ the downslope gravity component ε is varied, and within each figure the accumulation rate $\tilde{a}$ is varied according to (i) -5; (ii) 0; (iii) 0.03; (iv) 0.1; (v) $0.3\,\mathrm{m\,a^{-1}}$. Computations are for $\theta^{(b)} \in [\theta^{(s)}, 0]$. Zones in (Q_H, H)-space which are unstable are indicated by solid lines, stable flows by dotted lines. Sufficiently high downslope gravity components $(c–f)$ generate a fold catastrophe. The sign of $Q'_H(H)$ does not reliably determine stability.

equation discretization points in the ice and bedrock. Tests were made against solutions to the eigenvalue problem for the temperature equation, and the analytical Jacobian was checked against the numerical Jacobian.

4.1. *Cases with restricted coupling*

The uncoupled theory for the thickness evolution uncoupled in every way from temperature has eigenvalue given by $\lambda = -k_x^2 v - k_y^2 + \mathrm{i}k_x m$ (Nye 1959). Eigenvalues of the uncoupled temperature equation, with no horizontal advection, have been investigated in a glaciological context by Hanson & Dickinson (1988), who remind us that it is a Sturm–Liouville problem, implying the eigenvalues are real, and correspond to stable behaviour. Some similar computations, not reported in detail in this paper, extend this to cases where there is horizontal advection, heat flow in the bedrock, and dissipation by sliding or internal friction, but with rate factors which do not depend upon the temperature. There are some features of interest, in particular the way in which horizontal advection and lithospheric temperature variations introduce

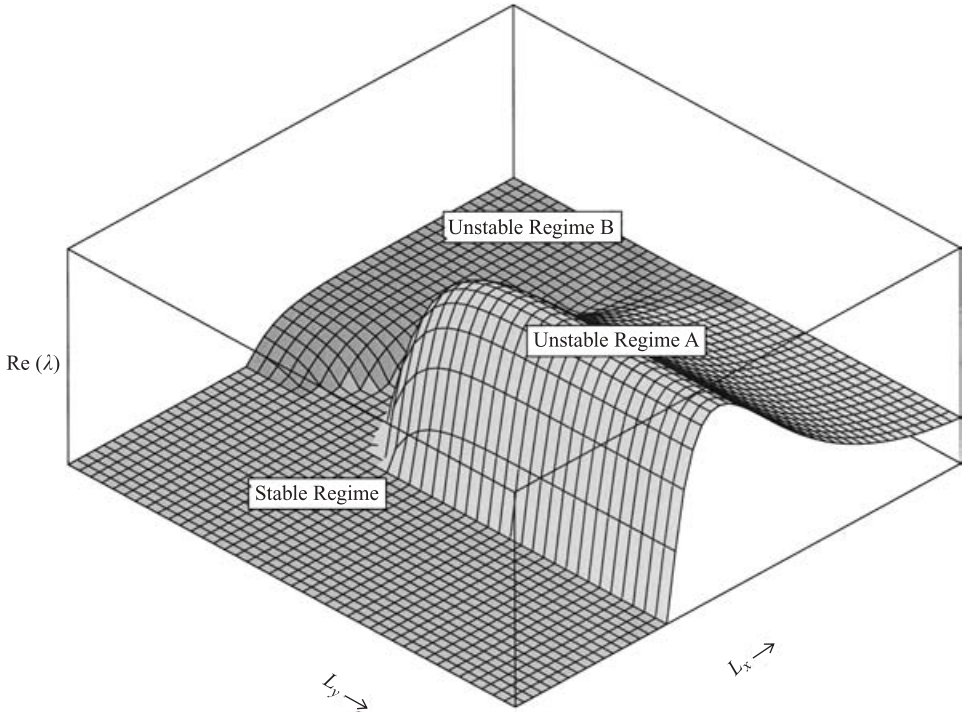

FIGURE 4. Sketch of surface showing the most positive real part of the eigenvalue as a function of surface wavelength (L_x, L_y). Typically, the surface is divided into three areas: Regime A, Regime B (both unstable regimes) and Stable Regime. Quantitative examples are provided in figure 5. Regime A shows strong dependence on longitudinal wavelength and weak dependence on transverse wavelength. Regime B has weak dependence on both wavelengths.

dispersion (i.e. the mode wave velocity depends on the wavenumber), and the strong coupling between the basal, conductive boundary layer and the bedrock in the slowest modes.

4.2. *Thermal coupling*

The results in this section refer to solutions to the eigenproblems set out in (2.10), (2.11), (2.12) and (2.13). This solution yields the eigenvalue λ, while the eigenfunctions comprise the triplet

$$E = (\hat{\theta}_{r1}(z), \hat{\theta}_1(\zeta), \hat{H}_1).$$

The eigenvalue problem is solved for wavenumber pairs $(\tilde{k}_x, \tilde{k}_y)$ corresponding to wavelengths $(\tilde{L}_x, \tilde{L}_y)$ ranging over $2\pi(0.2, 1000)$ km. Some of these cases correspond to situations where the shallow-ice approximation is no longer respected, but this turns out not to be crucial, as an asymptotic stability regime of the SIA is reached in these cases. The eigenvalue is a complex number, whose real component provides information about growth or relaxation of a mode, and whose imaginary component provides information about the wave speed of the mode. In all cases, the wave speed was positive, i.e. features are advected downstream. The discussion below refers to the real part of the eigenvalue, which indicates stability when it is negative.

Figures 4 and 5 illustrate features of the solution to the eigenproblem, for cases where flow is by internal deformation only. From inspection of many results, it is clear that a characteristic dependence of the most positive eigenvalue upon wavelength

emerges, which is sketched in figure 4. There is a stable regime which occurs for all transverse wavelengths and at relatively short longitudinal wavelengths. There is an unstable regime (Regime A) lying in the quarter of $(\tilde{L}_x, \tilde{L}_y)$-space where both transverse and longitudinal wavelengths are relatively large, where the growth rate depends on the longitudinal wavelength but only weakly on the transverse wavelength of the mode. Finally, there is a regime (Regime B) in the quarter of $(\tilde{L}_x, \tilde{L}_y)$-space where longitudinal wavelengths are relatively large and transverse wavelengths are relatively small, where the growth rate depends very weakly on both wavelengths. Regime B can be considered as a plateau. Some quantitative examples are shown in figure 5. The regimes are not all exhibited in their entireties in these plots, as sometimes the regime boundaries are at wavelengths outside the plots. Since growth rates in Regime A are higher than in Regime B, unstable systems near bifurcation exhibit only Regime A instabilities.

Figure 5 illustrates the most positive eigenvalue as a function of wavelength. It considers cases where $(\tilde{Q}_G, \tilde{\theta}^s) = (0.06\,\mathrm{W\,m^{-2}}, -25^\circ\mathrm{C})$, with indicated slope and accumulation, where the basal temperature is at melting point, and the thickness varies. Regime A instabilities are present in cases where the Regime B instabilities are absent. Regime B instabilities appear with the plateau already present. Time constants range from between ten years and one thousand years. The figure also plots, using colour coding, the quantity $\max(|\hat{H}|)/\max(|\hat{\theta}|)$ for each eigenvector corresponding to the unstable mode as a function of the wavelengths. In Regime B, this ratio is for all practical purposes zero, while for Regime A, values from 0.00 up to 0.04 are found. This corresponds to a roughly equal projection onto thickness and temperature, since the temperature scale factor selected is rather small (1 K compared with typical temperature variations of 25 K). This implies that Regime A instabilities have a roughly equal effect on thickness and temperature, while Regime B instabilities only operate on the temperature field.

Some of the internal deformation solutions were also computed in a configuration where no thermal coupling with the lithosphere was permitted (results not shown in detail). The linearized system was more unstable in the sense that bifurcations to instability occurred at lesser thicknesses, occurred in a greater region of parameter space and produced greater growth rates. Thus, thermal coupling with the lithosphere, whilst not affecting the qualitative dynamics, does affect its quantitative aspects.

Finally, the effect of sliding switching on around the melting point through the mechanism of a 'sliding activation energy' was considered. In the calculations reported here, the sliding velocity as a proportion of the total upper surface velocity was prescribed (either 0.5 or 0.9) and the sliding activation energy set to $\tilde{E}_s \in \{10^5, 10^6, 10^7\}$ J. The lowest activation energy is comparable with the activation energy for ice creep at melting point. These activation energy values correspond to ratios of sliding velocity at $\tilde{\theta}_m \pm 0.1$ K of $\{1.03, 1.4, 25\}$ respectively (keeping the stress constant). In the case where the activation energy is 10^5 J, the results were more or less the same as for the case of internal deformation. This indicates that from a dynamical point of view, the plug-flow asymptotics of Fowler (1992) are useful. Time constants were between a few centuries and around a thousand years. As the activation energy increases, time constants decrease to between 10 years or less ($\tilde{E}_S = 10^6$ J) and sub-annual ($\tilde{E}_S = 10^7$ J). The distinction in eigenvalue magnitude between Regime A and Regime B instabilities was no longer found, but when one considers the norm ratio $\max(|\hat{H}|)/\max(|\hat{\theta}|)$, the Regime A/Regime B distinction persists.

The physical causes of instability, and, equally importantly, damping can be investigated by removing terms from the perturbation equations. The most positive

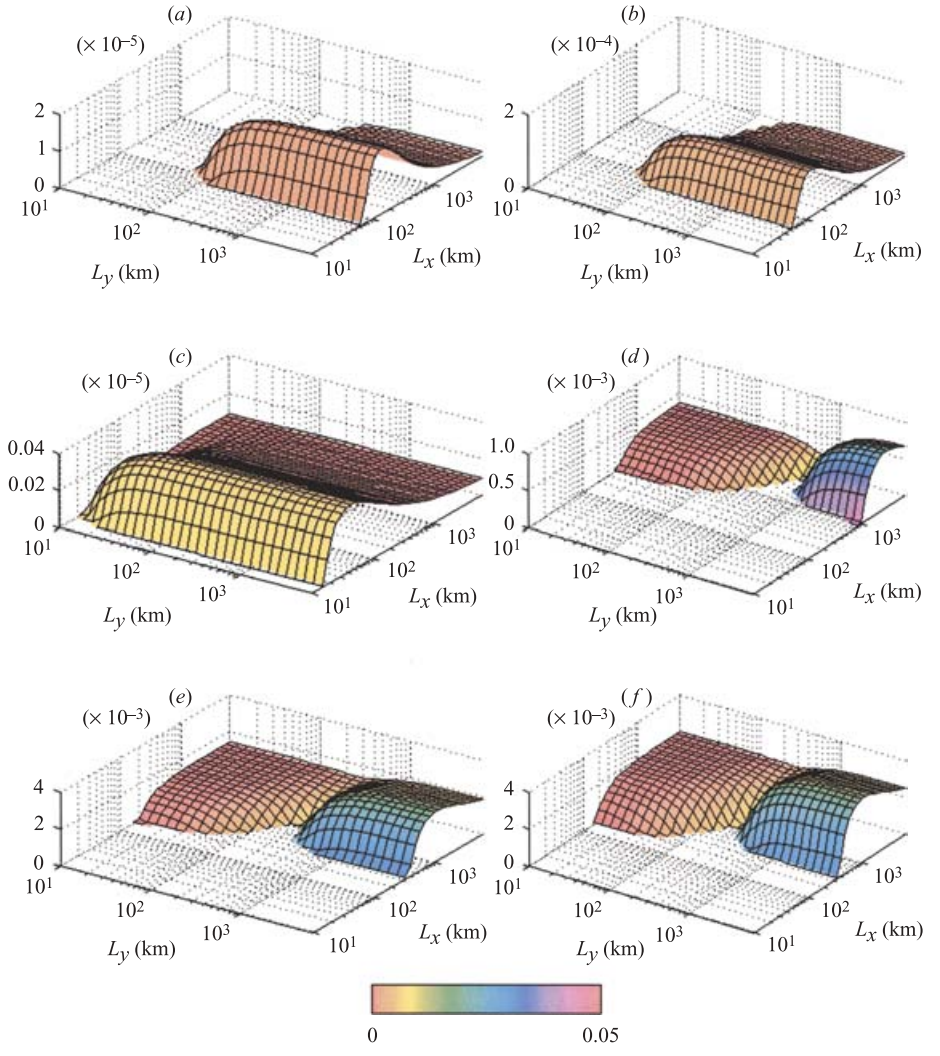

FIGURE 5. Surfaces showing the most positive eigenvalue $\tilde{\lambda}$ in a^{-1} as a function of surface perturbation wavelength (L_x, L_y). Studies are for the parameter set $(Q_G, \theta^{(s)}) = (0.06\,\mathrm{W\,m^{-2}}, -25^{\circ}\mathrm{C})$ and at $\theta_0^{(b)} = 0$ for: (*a*) $a = -5\,\mathrm{m\,a^{-1}}$, $\varepsilon = 0.005$; (*b*) $a = -5\,\mathrm{m\,a^{-1}}$, $\varepsilon = 0.01$; (*c*) $a = -5\,\mathrm{m\,a^{-1}}$, $\varepsilon = 0.1$; (*d*) $a = 0.1\,\mathrm{m\,a^{-1}}$, $\varepsilon = 0.005$; (*e*) $a = 0.1\,\mathrm{m\,a^{-1}}$, $\varepsilon = 0.01$; (*f*) $a = 0.3\,\mathrm{m\,a^{-1}}$, $\varepsilon = 0.01$. These diagrams show clearly the unstable Regimes A and B as well as the Stable Regime (figure 4). Colour coding shows $\max(|\hat{H}|)/\max(|\hat{\theta}|)$, for the eigenvector corresponding to the eigenvector with most positive real part. This shows the relative significance of thickness changes and temperature changes in this most unstable mode. Note that significant projection onto the thickness only occurs for longer transverse wavelengths: for shorter wavelengths, the instability is confined to the temperature field.

non-trivial eigenvalue for a number of alterations to the eigenproblem equations (2.10)–(2.13), and the perturbed flux definition (A 20), plotted as a function of wavelength, are shown in figure 6. These were for the case $(\tilde{Q}_G, \tilde{\theta}^s, \varepsilon, \tilde{a}) = (0.06\,\mathrm{W\,m^{-2}}, -25^{\circ}\mathrm{C}, 0.005, 0.3\,\mathrm{m\,a^{-1}})$ with the base of the ice at the melting point. Figure 6(i) is the full eigenproblem. The other figures have terms removed according to the corresponding labelling in the eigenproblem. Thus, in figure 6(iii), the eigenproblem

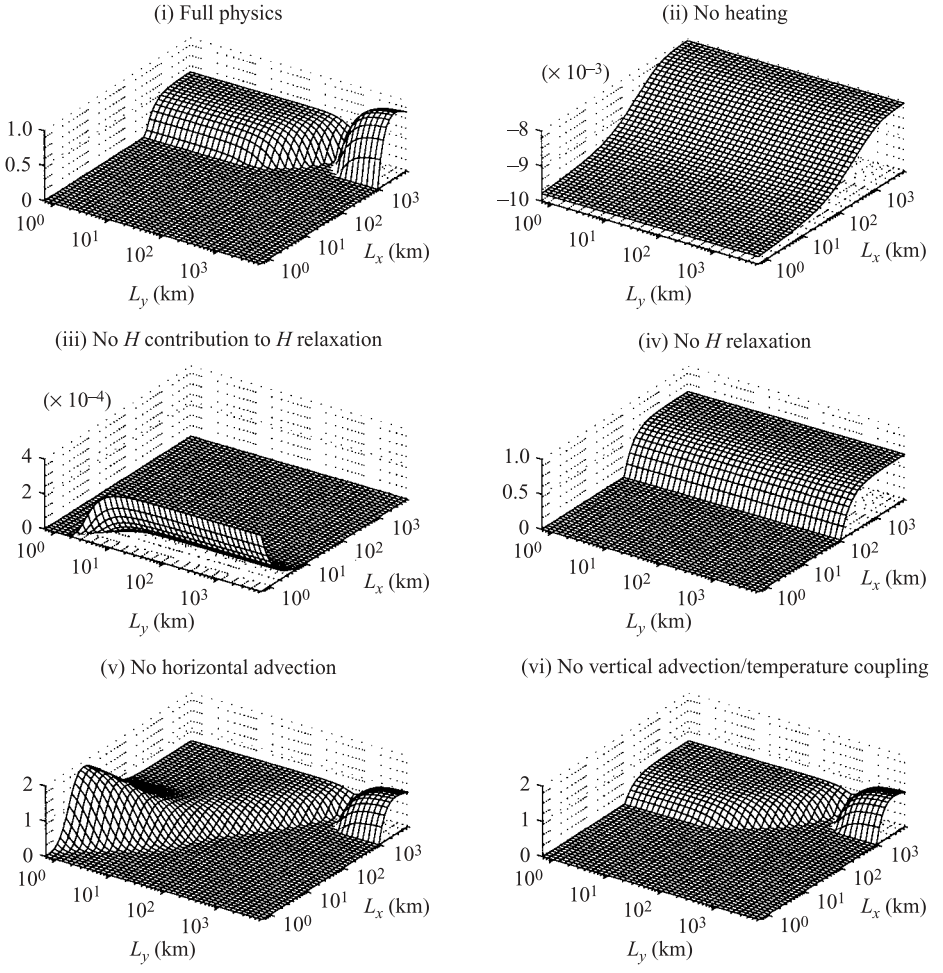

FIGURE 6. Surfaces showing the most positive eigenvalue $\tilde{\lambda}$ in a^{-1} as a function of surface perturbation wavelength (L_x, L_y). Studies are for the parameter set $(Q_G, \theta^{(s)}) = (0.06\,\mathrm{W\,m^{-2}}, -25^{\circ}\mathrm{C})$, for $a = 0.3$ and $\varepsilon = 0.005$ and at $\theta_0^{(b)} = 0$. The different cases have corresponding labelled terms removed from the eigenproblem set out in (2.10)–(2.13) and (A 20).

was altered by removing the term labelled (iii) in (2.10), while in figure 6(ii), the eigenproblem was altered by removing the terms labelled (ii) in (2.10), (2.11) and (2.12*a*). Case (i) is the true eigenproblem, against which all the other cases should be compared. In Case (ii) all the heating terms are removed, which completely stabilizes the flow, as expected. Case (iii) has the thickness self-decay term removed, showing that this term has a primary role in stabilizing flows at short wavelengths. In Case (iv), the effects of both temperature and thickness on thickness relaxation are removed. A notable feature is the y-independence of the stability diagram, showing that it is the evolving free surface that stimulates the lateral dependence. Case (v) has the horizontal advection term removed, which engenders further instabilities at short x and y wavelengths, indicating that horizontal advection stabilizes the flows at short wavelengths. Finally Case (vi) has the vertical advection/temperature coupling removed, again showing the role of advection in suppressing instability at shorter wavelength. (Note that to represent this case, the altered flux definition in (A 20) is

only used in the vertical advection term $\hat{\psi}_1$ in (2.14) and not to rederive the continuity equation (2.10).)

5. Discussion and conclusions

This paper has confirmed previous results (Nye 1971; Clarke *et al.* 1977) that thermally coupled flow of ice down an infinite plane is linearly unstable. These earlier studies did not consider finite horizontal wavelengths. The present study has extended these studies by explicitly demonstrating the dependence of the instability on horizontal wavelength with, for plane flow, a maximum growth rate at a finite, glaciologically relevant, wavelength. The rate constants for the instability are large enough at high slope (0.1) to suggest that surges of mountain glaciers, which occur over a few years (Paterson 1994) could be caused by thermal instabilities. By considering only the slower infinite wavelength instabilities, Clarke *et al.* (1977) reached the opposite conclusion. The present study supports computations that suggest that the Trapridge Glacier surges could be of thermal origin (Fowler, Murray & Ng 2001). The calculations confirm that the computed instabilities driving the fast, unstable phases of relaxation oscillations and surge-like phenomena can initiate at finite wavelengths, in regions where the ice is steeper (Payne 1995), and that the flow will restabilize and stagnate at low slopes which arise from exhaustion of the ice reservoir.

The normal-mode analysis results do not entirely correspond with a scalar analysis of the stability, in which the flux is supposed to be a scalar function of the thickness. In such an analysis, the sign of the derivative $\mathrm{d}Q_{\mathrm{H}}/\mathrm{d}H$ determines stability through the continuity equation $\partial_t H + \partial_x Q = a$. (Recall, $Q = Q(\boldsymbol{r}, t)$ and $Q = Q_{\mathrm{H}}(H)$.) To assess heuristically the stability of the scalar system one writes $\partial_t H + (\mathrm{d}Q_{\mathrm{H}}/\mathrm{d}H)\,\partial_x H = a$ and replaces this as a scale perturbation by $\dot{H} + (\mathrm{d}Q_{\mathrm{H}}/\mathrm{d}H)\,H = 0$. This is not rigorous, because the flux is a function of the temperature, thickness and slope, and these have associated decay time constants. The normal-mode analysis presented in this paper takes all of these factors into account, and shows that a negative $\mathrm{d}Q_{\mathrm{H}}/\mathrm{d}H$ is neither a necessary nor a sufficient condition for instability.

By using the technical device of a quasi-uniform flow, vertical advection has been considered self-consistently and found not to influence the qualitative dynamics significantly. The instability occurs whether the thermal inertia of the bedrock is considered or not, although the thermal properties of the bed do affect the quantitative aspects of the instability. Consideration of transverse undulations in the glacier surface reveals there to be two distinct wavelength regimes where unstable behaviour occurs. The location of these regimes in wavelength space depends upon the ice thickness, the bed slope, the surface temperature, the geothermal heat flux and the accumulation rate.

Regime A occurs for relatively longer *transverse* wavelengths, where there is a distinct maximum in the unstable eigenvalues at dimensionless *longitudinal* length scales between 1 and 10 (roughly speaking, between 100 and 1000 km). Regime A unstable mode eigenvectors have a reasonably strong projection on the thickness (i.e. unstable behaviour involves changes in the flow thickness). Regime A instabilities presumably disappear at a certain transverse wavelength, owing to the stabilizing effect of the transverse spreading of surface elevation. The wavelength below which transverse spreading dominates is not small, and is often greater than 100 km, an upper width for ice streams.

Regime B is in fact a plateau, occurring at relatively longer *longitudinal* wavelengths (again, very roughly, between 100 and 1000 km) and relatively shorter *transverse*

wavelengths, from a few tens of kilometres down to wavelengths comparable with the ice-sheet thickness. (At this wavelength, the SIA breaks down.) Regime B instabilities are generally in the region where $L_y \lesssim L_x$, and will therefore be manifested as the growth of elongated thermal structures aligned with the flow. Regime B instabilities do not have a strong projection onto the thickness, in other words the initial development of these features is in the temperature field, and a detailed inspection of the eigenfunctions shows that they project strongly onto the temperature field at the base of the ice, where of course the dissipation is greater. Regime B instabilities may even be ill-posed: if all modes grow at equal rates, the result is a random spatial field in the temperature, which contradicts assumptions in the model formulation. Horizontal conduction is expected to smooth short-wavelength features in the longitudinal direction.

These results can be encapsulated by asserting that there is weak mode selection of transverse wavelengths. There is no strongly preferred transverse wavelength at which instabilities grow. This means that even though in a technical sense long flow-parallel/short flow-transverse wavelength instabilities are predicted in this paper, it is not clear that stream-like features should necessarily develop. All the computations suggest that the bifurcation of the first unstable mode happens at very long transverse wavelengths. In neither of the regimes is there strong dependence of the unstable eigenvalue on the transverse wavelength. This means that the first unstable feature will be ribbing, and the development of this will drive the system from steady state. The linear stability of stream-like features in such regions of phase-space somewhat removed from equilibrium has not been analysed here. Whether there is mode selection in the transverse direction at larger amplitude might be revealed by a weakly nonlinear analysis. Mode selection might also be influenced by physics not included in the model formulation. Nonlinear calculations are needed to understand how the slower Regime B fingering instabilities in the temperature fields grow, how they manifest themselves in the thickness field and how they interact with the Regime A instability, which is always present before Regime B instabilities appear.

Some reasonable conjectures regarding the Regime A and Regime B instabilities can be made on the basis of the stability analyses of modified equations. The Regime A instabilities have a strong dependence on the free surface. The stabilization of this regime at relatively low longitudinal wavelengths is due to self-relaxation of thickness. In contrast, the eigenfunctions associated with Regime B fingering instabilities do not have a strong projection onto the thickness, and thus do not induce changes in the free surface. Since Regime B instabilities are not strongly coupled with thickness, the stabilization in the short-wavelength quadrant must come from x-derivative terms in the heat equation, which are horizontal advection or the dependence of the vertical velocity on the horizontal gradient of the rate factor and thence the temperature. In the parameter regimes considered the stabilization occurs at wavelengths too long for horizontal conduction to be important.

Some numerical models have computed spontaneous development of elongated features, aligned with the flow direction, bearing many similarities to ice streams, which arise as a result of thermoviscous coupling (e.g. Payne *et al.* 2000). If these are related to the Regime B instabilities, which do not strongly project onto thickness, one should note that present-day finite difference grids, while sampling Regime B instabilities, do not sample them over the whole range of wavelengths where instabilities occur. It is unlikely that these models properly describe the dynamics of the Regime B instabilities at the moment. Plane-flow numerical models (which perforce only represent Regime A instabilities), do in general exhibit instabilities which drive relaxation

oscillations. Payne (1995) describes computations where an instability is initiated in high-slope areas (see figure 3) and propagates backwards into the ice sheets – this appears to correspond to a Regime A instabilty. Regime A instabilities have a clearly defined maximum at longitudinal wavelengths (generally > 100 km) properly sampled by present-day models. If the fast phases of plane-flow relaxation oscillations reported by several authors are related to Regime A instabilities, one can have some confidence that they are being adequately resolved by these models. The recovery phase of a relaxation oscillation, which follows exhaustion of a reservoir, would correspond to low-slope, stable, slow-flowing ice-sheet geometries. Some discussion of the qualitative dynamics of thermally driven relaxation oscillations can be found in (Fowler *et al.* 2001). There is unlikely to be a simple relationship between the imaginary component of the eigenvalue and the presence of a relaxation oscillation.

Perhaps the most important conclusion is the weak lateral mode selection in thermoviscous instabilities. Since ice streams are of broadly consistent width (tens of kilometres) this suggests that the controls on their lateral dimensions do not stem from thermoviscous coupling. It is frequently suggested that some ice-stream locations do not have an obvious topographic control. However, there is a thickness control on flow stability. This means that a slight depression in the bedrock can trigger a local instability, and streamed flow. One might expect then some sensitivity to basal topography (e.g. Hulton & Mineter 2000), and weak topographic control leading to strong pattern formation. The enhanced ability of the ice stream to drain the ice implies that the stable areas will not thicken, and consequently remain stable.

Appendix. Derivation of the eigenvalue problem

A.1. *Momentum balance*

The standard (Hutter 1983; Morland 1984; Fowler 1992) shallow-ice approximation (SIA) is used, which expands the momentum-balance equations for slow creeping flow (2.1*c*) in terms of the aspect ratio $\tilde{H}_*/\tilde{L}_*$, which for convenience is set equal to ε, the ratio of the x- and z-components of gravity. After applying the scaling, the quasi-static formula for the shear stress is obtained as the asymptotic approximation

$$\tau_{xz} = -H(1-\zeta)(\partial_x s - 1) + O(\varepsilon^2), \tag{A 1a}$$

$$\tau_{yz} = -H(1-\zeta)\partial_y s + O(\varepsilon^2). \tag{A 1b}$$

The SIA also yields

$$\tau^2 \simeq \tau_{xz}^2 + \tau_{yz}^2. \tag{A 2}$$

By specifying $H_0 = 1$, the zeroth-order shear stresses are

$$(\tau_{xz0}, \tau_{yz0}) = (1, 0)(1-\zeta),$$

and first-order shear stresses in Fourier space are

$$(\hat{\tau}_{xz1}, \hat{\tau}_{yz1}) = (1 + \mathrm{i}k_x, \mathrm{i}k_y)(1-\zeta)\hat{H}_1. \tag{A 3}$$

The remaining stresses are not required. Basal tangential tractions are given by

$$\boldsymbol{T}_0^{(b)} = (1, 0), \tag{A 4a}$$

$$\hat{\boldsymbol{T}}_1^{(b)} = (1 + \mathrm{i}k_x, \mathrm{i}k_y)\hat{H}_1. \tag{A 4b}$$

The shallow-ice approximation also shows that $\boldsymbol{u}^{(b)} \simeq \boldsymbol{u}_{\parallel}^{(b)}$.

A.2. *Constitutive relations*

The ice is assumed to be below melting point for $z > b$. Flow of ice can occur by internal deformation according to the viscous relationship (2.2). The viscosity of ice ranges by three orders of magnitude in the temperature range typical of large ice sheets (Paterson 1994). The temperature dependence is modelled by a dual-Arrhenius relationship

$$R(\tilde{\theta}, \tilde{p}) = c_1 \exp(-\tilde{E}_1/\tilde{G}_c\tilde{\theta}) + c_2 \exp(-\tilde{E}_2/\tilde{G}_c\tilde{\theta}), \quad R(\tilde{\theta}_m, 0) \equiv 1, \tag{A 5}$$

where $\tilde{\theta}_m$ is the melting point of ice, $(c_1, c_2) = (3.7 \times 10^6, 5.4 \times 10^{26})$, the activation energies $(\tilde{E}_1, \tilde{E}_2) = (60, 140)$ kJ mol^{-1}, and $\tilde{G}_C = 8.314$ J mol^{-1} K^{-1} is the universal gas constant. This relationship is quantitatively similar to that proposed by Hooke (1981). The Clausius–Clapeyron constant is approximated as zero, which means that the pressure dependence of viscosity is ignored. When internal deformation is being treated, a useful choice of scale for the rate factor is

$$\tilde{A}_{c*} = 2\tilde{A}_c \bar{R}_0/(n+2), \tag{A 6}$$

which gives

$$A_c = (n+2)/(2\bar{R}_0). \tag{A 7}$$

This will be useful once the zeroth-order solution has been computed, as we can specify

$$\bar{R}_0 = \bar{R}(\theta_0). \tag{A 8}$$

Specification of a velocity scale

$$\tilde{u}_* = \tilde{A}_{c*}\tilde{H}_*^{n+1}\tilde{\rho}^n\tilde{g}^n\varepsilon^n, \tag{A 9}$$

gives a flux scale $\tilde{q}_* = \tilde{H}_*\tilde{u}_*$ that ensures $\boldsymbol{Q}_0 = (1, 0)$. The shear relationship under the SIA is

$$e_{\varkappa z} \simeq \tfrac{1}{2}\partial_z u_\varkappa, \qquad \partial_z u_\varkappa = (n+2)\frac{R}{\bar{R}_0}\tau^{n-1}\tau_{\varkappa z}, \qquad \varkappa = x, y. \tag{A 10}$$

Sliding is described by (2.4). Temperature dependence is expressed as

$$S(\tilde{\theta}, \tilde{p}) = \exp\left(-\frac{\tilde{E}_S}{\tilde{G}_C}\left(\frac{1}{\tilde{\theta}} - \frac{1}{\tilde{\theta}_m}\right)\right), \tag{A 11}$$

where $\tilde{E}_S$ is a sliding activation energy. Appropriate values of this are discussed where they are used. By construction $S(\tilde{\theta}_m, 0) = 1$. The activation energy is a descriptor of how quickly the sliding turns on as a result of temperature change. The 'sliding' can be regarded as a highly concentrated shear in the basal region (Fowler 1992), in which case it is reasonable to take the activation energy to be that of ice, and to have sliding occurring at sub-zero temperatures. The sliding activation energy can be used to simulate the way sliding is believed to increase around melting point; at this temperature the sliding switches on. There are also some arguments in favour of sub-zero sliding (Fowler 1986) as well as local sliding when the average temperature is below the melting point (Hughes 1998; Kleman *et al.* 1999).

When sliding is being considered, the horizontal velocity scale $\tilde{u}_*$ is selected to ensure a unit zeroth-order velocity, and the rate factor scale is then selected according to

$$\tilde{A}_s = \frac{S_0\tilde{u}_*}{\tilde{H}_*^n\tilde{\rho}^n\tilde{g}^n\varepsilon^n}, \tag{A 12}$$

which also gives

$$A_s S_0 = 1.$$

Again, S_0 is a choice of convenience, and will be defined as $S(\theta_0^b, 0)$. (This construction is not used in the perturbation. Computing a perturbed A_s using perturbed velocities is discussed and warned against by Hutter (1983, Chap. 4).

A.3. *Ice velocity and vertically integrated flux*

The flux $\boldsymbol{Q}$ and the partial flux $\boldsymbol{q}$ are defined by

$$\boldsymbol{Q} \equiv H \int_0^1 \boldsymbol{u}\, \mathrm{d}\zeta, \quad \boldsymbol{q} \equiv H \int_0^\zeta \boldsymbol{u}\, \mathrm{d}\zeta', \quad \boldsymbol{Q} \equiv \boldsymbol{q}\,(\zeta = 1),$$

where the prime indicates a dummy variable. When internal deformation is being considered, substitution of the approximate relationship (A 1) into (A 2), use of (A 10) and two integrations with respect to ζ yields the usual flux formulae associated with the shallow-ice approximation,

$$\boldsymbol{\Gamma} = [\partial_x s - 1, \partial_y s], \tag{A 13a}$$

$$\boldsymbol{Q} = -\frac{\bar{R}}{\bar{R}_0} H^{n+2} |\boldsymbol{\Gamma}|^{n-1} \boldsymbol{\Gamma}, \tag{A 13b}$$

$$\boldsymbol{q}(\zeta) = \frac{\bar{R}_q}{\bar{R}} \omega(\zeta)\, \boldsymbol{Q}, \tag{A 13c}$$

$$\omega(\zeta) \equiv \frac{(1-\zeta)^{n+2} + (n+2)\zeta - 1}{(n+2)(n+1)}, \tag{A 13d}$$

$$\bar{R}_q \equiv \frac{1}{\omega(\zeta)} \int_0^\zeta (\zeta - \zeta')(1-\zeta')^n R\, \mathrm{d}\zeta', \tag{A 13e}$$

$$\bar{R} \equiv (n+2) \int_0^1 (1-\zeta')^{n+1} R\, \mathrm{d}\zeta'. \tag{A 13f}$$

For sliding,

$$\boldsymbol{Q} = \boldsymbol{u}^b H = -\frac{S(\theta)}{S_0} H^{\ell+1} |\boldsymbol{\Gamma}|^{\ell-1} \boldsymbol{\Gamma}, \tag{A 14a}$$

$$\boldsymbol{q} = \zeta\, \boldsymbol{Q}. \tag{A 14b}$$

Usually, the two flow mechanisms are considered separately, but some computations have been carried out where both internal deformation and sliding occur, which require minor adjustments to the following development. A combined notation to represent internal deformation and sliding is

$$\nu = \begin{cases} n \\ \ell, \end{cases} \quad m = \begin{cases} n+2 \\ \ell+1, \end{cases} \quad C = \begin{cases} \dfrac{2}{n+2} A_c \bar{R} & \text{internal deformation} \\ A_s S & \text{sliding.} \end{cases} \tag{A 15}$$

The horizontal velocity is given by $\boldsymbol{u} = -C_u H^{m-1} |\boldsymbol{\Gamma}|^{\nu-1} \boldsymbol{\Gamma}$, where

$$C_u = \begin{cases} 2A_c \bar{R}_u & \text{internal deformation} \\ A_s S & \text{sliding,} \end{cases} \tag{A 16}$$

$$\bar{R}_u(\theta) \equiv \int_0^\zeta R(\theta)(1-\zeta')^n\, \mathrm{d}\zeta'. \tag{A 17}$$

If we choose (A 7) or (A 12) we obtain $C_0 = 1$,

$$\boldsymbol{Q}_0 = [1, 0], \quad \boldsymbol{q}_0 = \left[\frac{\bar{R}_q}{\bar{R}}\omega, 0\right]. \tag{A 18a, b}$$

Other zeroth-order quantities are not in general unity. The first-order velocities are given by

$$\boldsymbol{u}_0 = \begin{cases} \left((n+2)\,\dfrac{\bar{R}_u(\theta_0)}{\bar{R}_0}, 0\right) & \text{internal deformation} \\ (1, 0) & \text{sliding.} \end{cases} \tag{A 19}$$

The Fourier-transformed first-order fluxes are given by

$$\hat{q}_{1x}(\zeta)/|\boldsymbol{q}_0(\zeta)| = (m + v\mathrm{i}k_x)\hat{H}_1 + v\mathrm{i}k_x\hat{b}_1 + \overbrace{\mathscr{C}[\hat{\theta}_1;\zeta]}^{\text{(vi)}}, \tag{A 20a}$$

$$\hat{q}_{1y}(\zeta)/|\boldsymbol{q}_0(\zeta)| = \mathrm{i}k_y\hat{s}_1, \tag{A 20b}$$

$$\hat{\boldsymbol{Q}}_1 = \hat{\boldsymbol{q}}_1(1). \tag{A 20c}$$

In these relations, $\hat{b}_1$ represents a perturbation to the bed topography, and the square brackets indicate that $\mathscr{C}$ is a linear functional defined by

$$\mathscr{C}[\hat{\theta}_1;\zeta] = \begin{cases} \displaystyle\int_0^\zeta \frac{\dot{R}(\theta_0)}{R(\theta_0)}\hat{\theta}_1\,\mathrm{d}\zeta' & \text{internal deformation} \\ \dot{S}\left(\theta_0^b\right)\hat{\theta}_1^b & \text{sliding,} \end{cases} \tag{A 21}$$

where the dot over R and S indicates differentiation.

A.4. *Mass conservation*

The mathematical device of quasi-uniform flow, which allows mass supply through snowfall while retaining a horizontally uniform flow, implies a column-integrated conservation condition $\partial_t H + \nabla\cdot\boldsymbol{Q} = a$,, where a is the accumulation rate, with point conservation condition $\nabla\cdot\boldsymbol{u} + \partial_z w = 0$. The point continuity condition at zeroth and first order is

$$\partial_\zeta w_0 = -u_{0x}a_0/Q_{0x}, \tag{A 22}$$

$$\partial_\zeta w_1 + \nabla\cdot\boldsymbol{u}_1 + \partial_\zeta u_0 \mathrm{i}k_x(\zeta H_1 + b_1) = 0. \tag{A 23}$$

The construction maintains the normalized vertical velocity distribution found in the shallow-ice approximation, since necessarily $\partial_x u_{0x} \propto u_{0x}$ and continuity implies $\partial_\zeta w_0 = -u_{0x}a_0/Q_{0x}$. The first-order continuity equation in Fourier space is

$$\lambda\hat{H}_1 - \mathrm{i}\boldsymbol{k}\cdot\hat{\boldsymbol{Q}}_1 = \hat{a}_1, \tag{A 24}$$

The expression for $\hat{\boldsymbol{Q}}_1$ (A 20) is inserted in this equation to obtain the thickness evolution equation (2.10).

A.5. *Heat balance*

Using the scaling of Morland (1984), applying the shallow-ice approximation, transforming into the normalized coordinate system, and then following the development of Hindmarsh (1999) to write the vertical velocity in terms of the

flux gradient, allows the heat equations (2.1*f–k*) to be written as

$$\partial_t\theta + \boldsymbol{u}\cdot\nabla_{\mathrm{H}}\theta + \frac{\psi}{H}\partial_\zeta\theta = \frac{\beta}{H^2}\partial_\zeta^2\theta + \alpha D, \qquad 0 \leqslant \zeta \leqslant 1, \tag{A 25a}$$

$$\psi \equiv \zeta\nabla\cdot\boldsymbol{Q} - \nabla\cdot\boldsymbol{q} - \zeta a, \tag{A 25b}$$

$$\theta^{(s)} - \gamma s = 0, \qquad \zeta = 1, \tag{A 25c}$$

$$-\partial_\zeta\theta = \varpi(\boldsymbol{T}^b\cdot\boldsymbol{u}^b - K_r\partial_z\theta_r), \qquad \zeta = 0, \tag{A 25d}$$

$$\partial_t\theta_r = \kappa_r\partial_z^2\theta_r, \qquad z < b, \tag{A 25e}$$

$$-K_r\partial_z\theta_r = Q_G, \qquad z \to -\infty, \tag{A 25f}$$

where as before the dimensionless field variables defined within the ice are functions of ζ, the thermal conductivities of ice and rock are K_i and K_r, and D represents the shallow-ice approximation of the heating due to internal dissipation given by

$$D = H^{-1}(1-\zeta)\,\partial_\zeta\boldsymbol{u}\cdot\boldsymbol{T}^{(b)}. \tag{A 26}$$

Equation (A 25*a*) is the heat equation, the third term on the left-hand side representing the vertical advection; (A 25*b*) is the vertical velocity in the normalized coordinate system; (A 25*c*) is the upper surface prescribed temperature; (A 25*d*) is the heat-flux boundary condition in the ice at the base, which include sliding heating; (A 25*e*) is the heat equation in the bedrock; and (A 25*f*) is the flux boundary at depth in the bedrock. Thus, following Ritz (1987), temperature variations within the lithosphere $z < b$, modelled as a half-space, are included; θ_r represents the temperature in the bedrock, κ_r is the thermal diffusivity of rock and Q_G is the geothermal heat flux. The dimensionless parameters are given by

$$\beta \equiv \frac{\tilde{\kappa}}{\tilde{H}_*\tilde{a}_*}, \quad \beta_r \equiv \frac{\tilde{\kappa}_r}{\tilde{H}_*\tilde{a}_*}, \quad \alpha \equiv \frac{\tilde{g}\tilde{H}_*}{\tilde{c}\tilde{\theta}_*}, \quad \varpi \equiv \varepsilon\tilde{\rho}\tilde{g}\frac{\tilde{H}_*^2\tilde{u}_*}{\tilde{K}_i\tilde{\theta}_*}. \tag{A 27}$$

Linearization of the heat equation gives (2.9) at zeroth order, where the scaling constructions $H_0 \equiv 1$, $\boldsymbol{T}_0^{(b)} = [1, 0]$ have been used. At first order, the linearization yields (2.11)–(2.13). This completes the description of the eigenproblem.

REFERENCES

Balmforth, N. J. & Craster, R. V. 2001 Dynamics of cooling domes of viscoplastic fluid. *J. Fluid. Mech.* **422**, 225–248.

Bamber, J. L., Vaughan, D. G. & Joughin, I. R. 2001 Widespread complex flow in the interior of the Antarctic ice sheet. *Science* **287**, 1248–1250.

Clarke, G. K. C., Nitsan, U. & Paterson, W. S. B. 1977 Strain heating and creep instability in glacier and ice sheets. *Rev. Geophys. Space Phys.* **15**, 235–247.

Davis, S. H. 2000 Interfacial fluid dynamics. In *Perspectives in Fluid Dynamics* (ed. G. K. Batchelor, H. K. Moffatt & M. G. Worster). Cambridge Universtiy Press.

Fowler, A. C. 1986 Sub-temperate basal sliding. *J. Glaciol.* **32**, 3–5.

Fowler, A. C. 1987*a* Sliding with cavity formation. *J. Glaciol.* **33**, 255–267.

Fowler, A. C. 1987*b* A theory of glacier surges. *J. Geophys. Res.* **92**(B9), 9111–9120.

Fowler, A. C. 1992 Modelling the dynamics of ice sheets. *Geophys. Astrophys. Fluid Dyn.* **63**, 29–66.

Fowler, A. C. & Johnson, C. 1996 Ice-sheet surging and ice-stream formation. *Ann. Glaciol.* **23**, 68–73.

Fowler, A. C. & Larson, D. 1980*a* The uniqueness of steady state flows of glaciers and ice sheets. *Geophys. J. R. Astron. Soc.* **63**, 333–345.

Fowler, A. C. & Larson, D. 1980*b* Thermal stability properties of a model of glacier flow. *Geophys. J. R. Astron. Soc.* **63**, 333–345.

Fowler, A. C., Murray, T. & Ng, F. S. L. 2001 Thermally controlled glacier surging. *J. Glaciol.* **47**, 527–538.

Glen, J. W. 1955 The creep of poly-crystalline ice. *Proc. R. Soc. Lond.* A **226**, 519–538.

Greve, R. & MacAyeal, D. R. 1996 Dynamic/thermodynamic simulations of Laurentide ice-sheet instability. *Ann. Glaciol.* **23**, 328–335.

Hanson, B. & Dickinson, R. E. 1988 A transient temperature solution for borehole model testing. *J. Glaciol.* **33**, 140–148.

Hindmarsh, R. C. A. 1997 Normal modes of an ice-sheet. *J. Fluid Mech.* **335**, 393–413.

Hindmarsh, R. C. A. 1999 On the numerical computation of temperature in an ice-sheet. *J. Glaciol.* **45**, 568–574.

Hindmarsh, R. C. A. 2001 Influence of channelling on heating in ice-sheet flows. *Geophys. Res. Lett.* **28**, 3681–3684.

Hindmarsh, R. C. A. & Hutter, K. 1988 Numerical fixed domain mapping solution of free surface flows coupled with an evolving interior field. *Intl J. Numer. Anal. Meth. Geomech.* **12**, 437–459.

Hooke, R. LeB. 1981 Flow law for polycrystalline ice in glaciers: Comparison of theoretical predictions, laboratory data, and field measurements. *Rev. Geophys. Space. Phys.* **19**, 664–672.

Hooper, A. P. & Boyd, W. G. C. 1983 Shear-flow instabilty at the interface between two viscous fluids. *J. Fluid Mech.* **128**, 507–528.

Hughes, T. J. 1998 *Ice Sheets.* Oxford University Press.

Hulton, N. R. J. & Mineter, M. 2000 Modelling self-organization in ice streams. *Ann. Glaciol.* **30**, 127–136.

Hutter, K. 1983 *Theoretical Glaciology*. Reidel.

Kleman, J., Hättestrand, C. & Clarhäll, A. 1999 Zooming in on frozen bed patches: scale dependent controls on Fennoscandian ice sheet basal thermal zonation. *Ann. Glaciol.* **28**, 189–194.

MacAyeal, D. R. 1992 Irregular oscillations of the West Antarctic Ice Sheet. *Nature* **359**, 29–32.

MacAyeal, D. R. 1993 A low-order model of growth/purge oscillations of the Laurentide ice-sheet. *Paleoceanography* **8**, 767–773.

Marshall, S. J. & Clarke, G. K. C. 1997 A continuum mixture model of ice stream thermo-mechanics in the Laurentide Ice Sheet 2. Application to the Hudson Strait Ice Stream. *J. Geophys. Res.* **102** (B9), 20615–20637.

Morland, L. W. 1984 Thermo-mechanical balances of ice sheet flows. *Geophys. Astrophys. Fluid Dyn.* **29**, 237–266.

Nye, J. F. 1959 The motion of ice sheets and glaciers. *J. Glaciol.* **3**, 493–507.

Nye, J. F. 1971 Causes and mechanics of glacier surges: a discussion. *Can. J. Earth Sci.* **8**, 306–307.

Oron, A., Davis, S. H. & Bankoff, S. G. 1997 Long-scale evolution of thin liquid films. *Rev. Mod. Phys.* **69**, 931–980.

Paterson, W. S. B. 1994 *The Physics of Glaciers*, 3rd Edn. Pergamon.

Pattyn, F. 1996 Numerical modelling of a fast-flowing outlet glacier: experiments with different basal conditions. *Ann. Glaciol.* **23**, 237–246.

Payne, A. J. 1995 Limit cycles in the basal thermal regime of ice sheets. *J. Geophys. Res.* **100** (B3), 4249–4263.

Payne, A. J. & Dongelmans, P. 1997 Self-organization in the thermomechanical flow if ice-sheets. *J. Geophys. Res.* **102** (B6), 12219–12233.

Payne, A. J., Huybrechts, P., Abe-Ouchi, A. *et al.* 2000 Results from the EISMINT intercomparison: the effects of thermo-mechanical coupling. *J. Glaciol.* **46**, 227–238.

Reisfeld, B. & Bankoff, S. G. 1992 Nonisothermal flow of a liquid-film on a horizontal cylinder. *J. Fluid Mech.* **236**, 167–196.

Ritz, C. M. 1987 Time-dependent boundary conditions for calculation of temperature fields in ice-sheets. In *The Physical Basis of Ice-sheet Modelling* (ed. E. D. Waddington & J. S. Walder). IAHS Publication 170, pp. 207–216.

Yih, C. S. 1967 Instability due to viscosity stratification. *J. Fluid Mech.* **27**, 337–352.

Yuen, D. A., Saari, M. R. & Schubert, G. 1986 Explosive growth of shear-heating instabilities in the down-slope creep of ice. *J. Glaciol.* **32**, 314–320.

Yuen, D. A. & Schubert, G. 1979 The role of shear heating in the dynamics of ice-sheets. *J. Glaciol.* **23**, 170–177.